**Future Energy**
**Open Access Journal**
ISSN 2832-0328

November 2026| Volume 05 | Issue 04 | Pages 12-17

Journal homepage: https://fupubco.com/fuen

https://doi.org/10.55670/fpll.fuen.5.4.2

Future Publishing LLC

Article

# Effect of Ni-additive on jute stick charcoal-mediated carbon anode of Li-ion batteries

**Tauhidul Hossain, Md. Arafat Rahman*, Konok Chandra Bhowmik, Rudra Barua**

Department of Mechanical Engineering, Chittagong University of Engineering & Technology, Chittagong, Bangladesh

**ARTICLE INFO**

*Article history:*
Received 29 April 2026
Received in revised form
26 July 2026
Accepted 22 August 2026

Keywords:
Anode, Li-ion batteries, Jute stick, Charcoal, Amorphous carbon, Nickel nanoparticle

*Corresponding author
Email address:
arafat@cuet.ac.bd

DOI: 10.55670/fpll.fuen.5.4.2

**ABSTRACT**

Li-ion batteries (LIBs) have gained popularity as a potential device for sustainable energy transition. Because of its simple and environmentally benign production, biomass-derived amorphous carbon is a viable anode for LIBs as a possible replacement for graphite. However, its performance is limited by structural deterioration and low conductivity. Therefore, developing low-cost biomass-derived carbon anodes with improved electrical conductivity and cycling stability is important for sustainable LIB applications. Here, slow pyrolysis has been used to produce amorphous carbon from jute stick charcoal. The jute sticks were pyrolyzed at 400 °C, and the structural characterization confirmed the successful formation of amorphous carbon with flake-like porous morphology. The resulting carbon was evaluated as an anode material in a full cell. After 500 cycles, this anode demonstrated a discharge capacity of 125.46 mAh/g and a Coulombic efficiency (CE) of 68.4% at 1C. In addition, Ni metal powder additives were added to improve cell performance. Ni considerably reduced the cell impedance and enhanced electrode conductivity. As a result, after 500 cycles, the Ni-added anode demonstrated improved performance with a discharge capacity of 148.02 mAh/g and a CE of 73% at 1C. Electrochemical investigations further indicated reduced cell resistance after Ni incorporation, demonstrating enhanced electronic conduction and interfacial charge-transfer kinetics.

## 1. Introduction

Eco-friendly energy storage devices are necessary for the sustainable energy transition due to the scarcity of fossil fuels, rising $CO_2$, and the intermittency of renewable energy [1]. LIBs are widely used in portable electronic gadgets, hybrid electric vehicles, and developing smart grids because they are among the most effective and ecologically friendly energy storage technologies [2]. The most popular anode in commercial Li-ion batteries is graphite, an allotrope of carbon [3]. Although graphite forms naturally at a somewhat lower temperature of 450–600 °C, this process requires a synergistic natural process that includes temperature, pressure, shear strain, and metamorphic time [4]. In practice, producing graphite from both organic and inorganic precursors requires either high-temperature treatment at 1000–3000 °C or a complex chemical process [5]. In addition, graphite has a low theoretical capacity of 372 $mAhg^{-1}$ and a strict rated capacity [6], which is the reason researchers are trying to improve the structural mechanism of graphite in order to improve the electrochemical performance of anodes, as well as finding a suitable candidate to replace graphite commercially, which will rely more on green manufacturing and reduce the production cost. Researchers are therefore interested in less expensive, non-toxic manufacturing of carbon anodes. Huong et al. [7], for example, created a nanocarbon from coal that demonstrated a discharge capacity of 336 mAh/g at 0.1C. Pyrolysis of biomass carbon produces amorphous carbon with three-dimensional crosslinks, which is important for the shift to sustainable energy due to its simple synthesis and environmental friendliness. One of the main structural elements of jute sticks is lignin, a naturally occurring polymer with a high carbon content (>60%) that serves as a precursor to amorphous carbon networks [8]. In most cases, amorphous carbon has a larger specific capacity than graphite, but it degrades rapidly over cycling in a full cell, and the material loses conductivity and structural integrity. Pham et al. [9] synthesized $SiO_2$/C anode from rice husk and incorporated it in a full cell, which delivered a low discharge capacity of 114.2 $mAhg^{-1}$, which degraded very quickly in the following cycles. Jiang group [10] synthesized 3D rod-like carbon nanostructure from ramie fiber (RFC) and 2D carbon nanosheets from corncob (CC). The RFC anode delivered a high initial specific capacity of 757 mAh/g, but it suddenly dropped to 432 mAh/g in the next cycle and decreased further in consecutive cycles. The CC anode also exhibited a similar trend in their investigation. Both anodes lasted less

than 200 cycles. Therefore, amorphous hard carbons derived from biomass wastes should be further investigated in order to improve their electrochemical performance, stability, and electrical conductivity as negative electrodes of LIBs. To develop a sustainable biomass-based anode for LIBs, materials of high specific capacity and good rate capability are still needed. In this context, the conductivity of several anode materials has been reported to be improved by metals or metal oxides such as Ni, Cu, $WO_3$, $Fe_3O_4$, etc [11-14]. However, reports on the effectiveness of these metals in improving the performance of different biomass-based hard amorphous carbons remain insufficient to this day. To better understand the effectiveness of additive metals on the conductivity of biomass-based amorphous carbons, more biomass materials should be investigated with these additives. Moreover, almost all studies have reported high-temperature pyrolysis or hydrothermal carbonization as the main synthesis route for valorizing hard carbons from biomass [15-17], which raises concerns about energy consumption, toxicity, and cost-effectiveness. In this study, we conducted slow pyrolysis of jute sticks to create amorphous carbon for Li-ion battery anodes. To examine the impact of Ni on electrochemical performance, we added Ni metal powder to the carbon anode materials and thoroughly analyzed the resulting materials using galvanostatic testing, cyclic voltammetry, and electrochemical impedance spectroscopy. The objective is to investigate the effect of metallic Ni addition on the electrochemical performance and cycling stability of jute stick charcoal-derived amorphous carbon as an anode material for lithium-ion batteries.

## 2. Experimental details

### 2.1 Anode fabrication

First, locally available dry jute sticks were collected. They were cleaned with tap water and then rinsed several times with distilled water. After that, the washed sticks were kept in a closed, dark room for two days to dry. The sticks were then broken into small pieces and stored in a steel pot. The pot was sealed tightly and heated at 400 °C for five hours. A mortar and pestle were used to grind the resultant charcoal. The charcoal particles were filtered using a sieve. These amorphous carbon particles were used to fabricate the anode. After that, powdered Ni metal was added as an additive. In this paper, charcoal-mediated amorphous carbon is denoted as a-C, and Ni-added amorphous carbon is denoted as a-C-Ni. A 90 wt% a-C and 10 wt% poly(vinylidene fluoride) (PVDF) binder mixture was made for the a-C anode. A mixture of 70 wt% a-C, 20 wt% metallic Ni powder, and 10 wt% PVDF binder was made for the a-C-Ni anode. To prepare a homogeneous mixture, we ball-milled both combinations for 15 minutes at 200 rpm. After adding a small amount of N-methyl-2-pyrrolidone, we prepared homogeneous slurries. The slurries were then cast onto Cu foil and heated overnight at 105 °C. We obtained ~95 μm of active material coating on Cu foil.

### 2.2 Cell assembly

From the fabricated slurry-coated Cu foil, round discs 15 cm in diameter were cut. Cells were fabricated in a CR2032 casing using one disc as the anode, a polyvinyl chloride separator (18 cm), and a $LiCoO_2$ cathode (15 cm diameter). The electrolyte was 1 M LiPF6 in an ethylene carbonate: diethylene carbonate (3:7) solution. Following assembly, the cells were crimped at 80 psi.

### 2.3 Characterization

Scanning electron microscopy (SEM) images were taken using a JEOL JSM-7600F. The same instrument was used for Energy Dispersive X-ray Spectrometry (EDS) at 5 kV. Attenuated total reflectance Fourier Transform Infrared (FTIR) spectroscopy was conducted for mixtures of active materials and PVDF binder in the 400- 4500 cm−1 range using the PerkinElmer FTIR Spectrometer with a force gauge of ~85.

### 2.4 Electrochemical tests

Galvanostatic charge-discharge (GCD) was performed in the range of 0- 2.5 V (vs. Li/Li+). A CS100 potentiostat was used to perform electrochemical impedance spectroscopy and cyclic voltammetry. All CVs had a potential window of 0.1-3.0 V (vs. Li/Li+) at a scan rate of 5 mV/s, and all EIS analyses were conducted between 100 kHz and 0.01 Hz.

## 3. Results & discussion

### 3.1 Characterization

Figure 1 shows the SEM images of a-C particles. The images indicate irregular plate-like morphologies with uneven thickness. We noticed a high aspect ratio and edge defects in the plate-like particles. Edge defects were observed. These defects may result from ball milling. In addition, defect-rich amorphous carbon flakes are developed due to partial preservation of the lignocellulosic framework of the jute stick. As Li storage sites, the increased exposed surface and inter-plate porosity are advantageous.

Figure 1c shows EDX spectra of a-C-Ni. A distinct C Kα peak at about 0.27 keV was observed, indicating the presence of carbon. Likewise, the presence of Ni is confirmed by the Ni L (~0.85–0.90 keV), Ni Kα (~7.47 keV), and Ni Kβ (~8.26 keV) peaks. For each sample, the FTIR spectra (Figure 2) show a wide transmittance band in the 3600–3000 $cm^{-1}$ range. This shows the O-H stretching resulting from the samples' moisture level. Skeletal C=C vibrations of $sp^2$-bonded amorphous carbon are shown by the strong, sharp peak at around 1600 $cm^{-1}$ [18]. The band at 1400–1200 $cm^{-1}$ could be explained by carbon particle surface flaws brought on by the C–O functional group. The aliphatic C–H and $CF_2$ stretching vibrations of PVDF are shown by the weak band at 3000–2850 $cm^{-1}$ and the sharp, strong band at 1200–1100 $cm^{-1}$ [19]. Nevertheless, since metallic particles are not infrared active, no band corresponds to them.

### 3.2 Galvanostatic charge-discharge

To better represent the cycling performance of the two anodes, Figure 3 shows the voltage-current profiles of only the first and last 5 cycles. Careful observation of the voltage profile reveals voltage hysteresis. The charging profile was higher than the discharging profile, suggesting that the anode cannot supply the same amount of charge that was stored during charging. Thus, more energy is required during charging, and less energy is obtained during discharge.

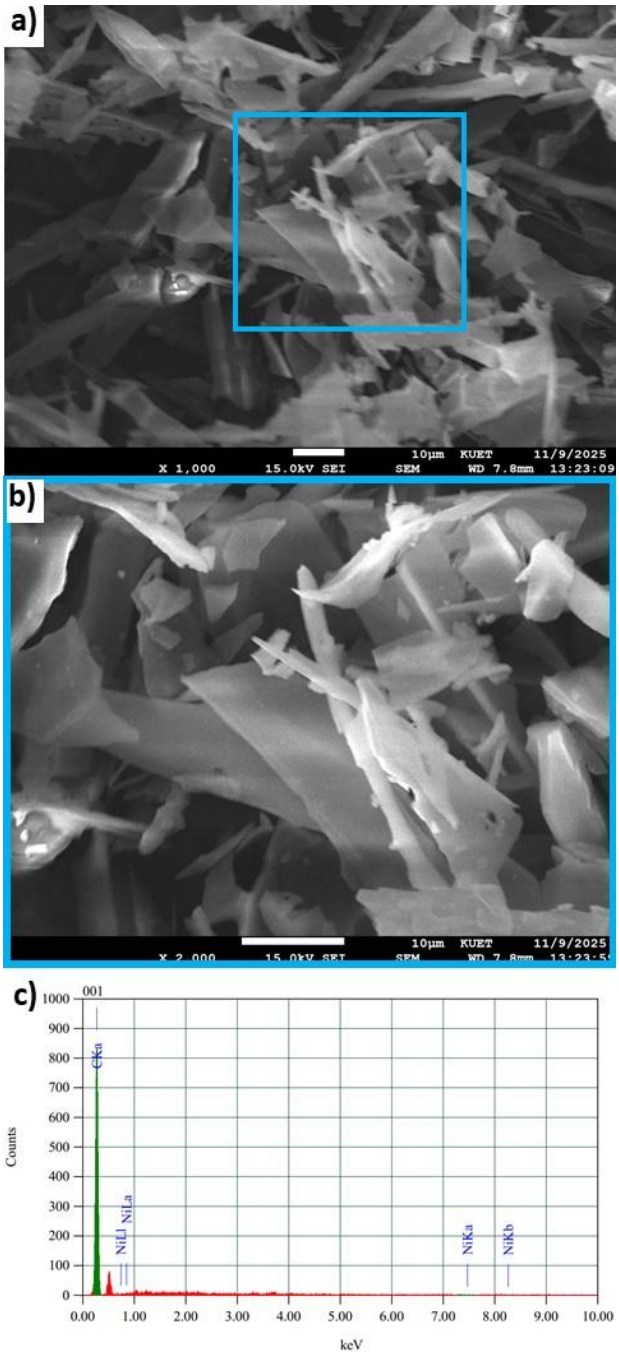


**Figure 1.** Characterization of jute stick charcoal-mediated carbon. a,b) SEM images of a-C particles, and c) EDX spectra of a-C-Ni

We noticed no abrupt, fast changes in the voltage profile during the charge-discharge transition. This incident typically indicates a delayed electrochemical response of the a-C anode. The increase in polarization throughout cycling is observed in the smaller voltage-current profile at the end of the cycles. Nevertheless, Ni addition improved cycling performance. Over 500 cycles, the voltage profile of a-C-Ni showed minimal hysteresis and consistent cut-off voltages (Figure 3b). Furthermore, the current profile was superior to that of the a-C anode.

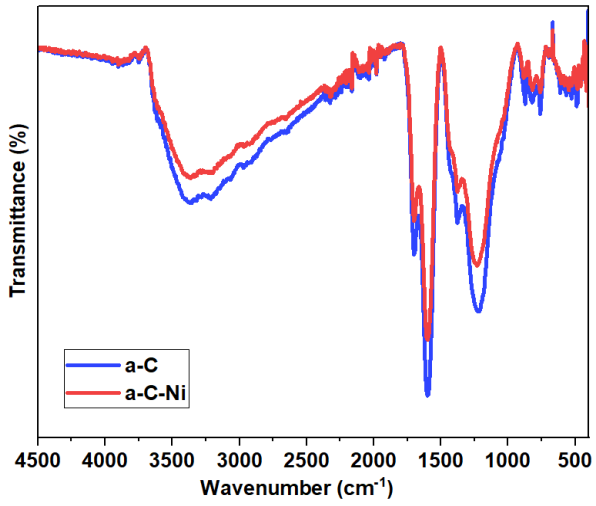


**Figure 2.** FTIR spectra of a-C and a-C-Ni

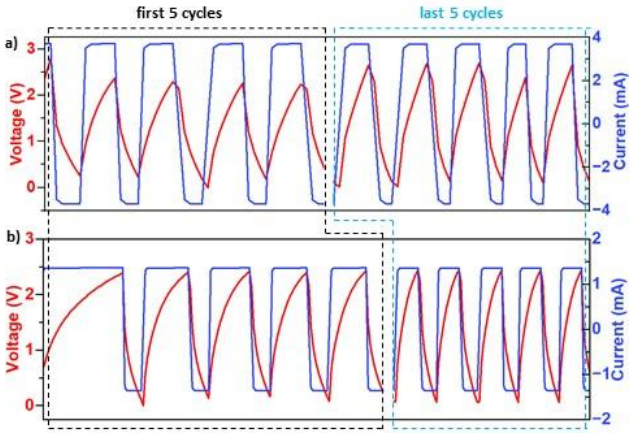


**Figure 3.** Voltage and current profile of the first and last 5 cycles of 500 GCD cycles: a) a-C and b) a-C-Ni

The strong peaks in the voltage profile during the charge-discharge transition indicate a better electrochemical response of the C-Ni anode, even though Fig. 3b shows poorer discharge ability compared with the stored charge as before. Although polarization still occurs at the end of the cycles, the voltage-current profile shows good reversibility. Although the voltage hysteresis and delayed electrochemical response were eliminated, the Ni additive could not prevent the increase in polarization. The electrochemical cycling performance of each anode after cycling is displayed in Figure 4. Figure 4 depicts the discharge capacity and CE for each corresponding cycle. The a-C anode demonstrated a first-cycle discharge capacity of 137.75 mAh/g (Figure 4a). The anode showed consistent cycling for the first 150 cycles, with discharge capacities ranging from 137.75-172.19 mAh/g, respectively. After 150 and 300 cycles, respectively, we observed modest and moderate capacity fading. For the last 50 cycles, the average discharge capacity was 125.46 mAh/g. Since Li entrapment is frequent in amorphous carbon, the capacity fading may be caused by the permanent loss of Li [20].

CE is referred to as the ratio of discharge capacity to charge capacity in a particular cycle [21]. This CE signifies the extent of parasitic side reactions (PSRs) in each cycle and ultimately in the overall cycling [22]. The CE of the first cycle was 66.67%, and the CE for the last 50 cycles was 68.4%. The CE clearly indicates a loss of Li inventory stored during charging. The low CE indicates PSR and Li entrapment during initial cycles. However, the CE improves a little over 500 cycles, indicating a slight reduction in Li entrapment and PSRs. However, the cell impedance may rise over cycling. In Figure 4b, we noticed improved electrochemical performance of the a-C-Ni anode. The initial discharge capacity was 172.27 mAh/g. No significant capacity fading was noticed over the first 50 cycles.

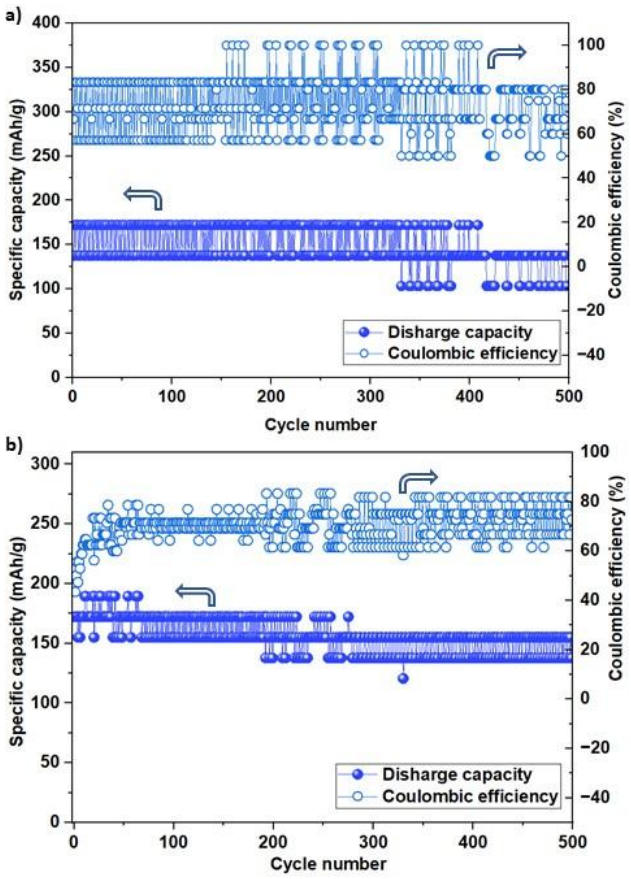


**Figure 4.** Electrochemical cycling performance: discharge capacity and Coulombic efficiency of a) a-C and b) a-C-Ni

Over the first 200 cycles, the discharge capacity remained almost constant, with minimal variation. For the last 50 cycles, the average discharge capacity was 148.02 mAh/g. As a result, C-Ni performs better than C and C-Cu anodes. The initial CE was 43.38%, and for the last 50 cycles, it was 73%, indicating a significant rise in CE. Although fluctuations were observed in the final 50 cycles, there was no discernible decline in CE. Thus, the PSRs and Li entrapment reduced upon cycling, signifying enhanced electrochemical performance of a-C-Ni. Ni increased the anode's conductivity and reduced polarization rather than blocking Li storage sites [23].

### 3.3 Electrochemical impedance spectra

The EIS spectra for each anode under different cell conditions are shown as Nyquist plots (Figure 5). Figure 5c shows the corresponding fitted equivalent circuit for the EIS spectra. For the bulk anodes, we are considering bulk resistance (Rb). The interface resistance is regarded as RSEI. $R_{ct}$ is the charge transfer resistance. Rb, RSEI, and $R_{ct}$ are associated with the high-, mid-, and low-frequency ranges, respectively. The combined resistance of RSEI and $R_{ct}$ is considered the polarization resistance. The depressed semicircle indicates non-ideal capacitive behavior originating from surface heterogeneity and is represented as a constant phase element, Q [24].

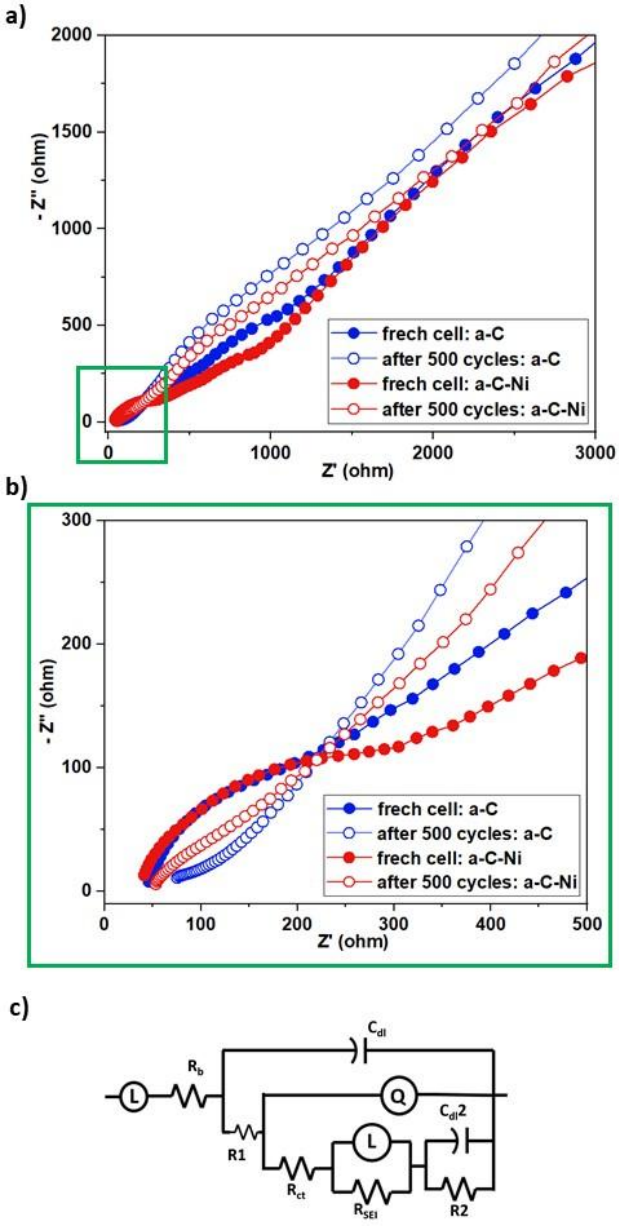


**Figure 5.** Electrochemical impedance spectra of a,b) a-C and a-C-Ni, and c) corresponding equivalent circuit

Figure 6 shows the corresponding numerical values for the anodes at different cell conditions. Figure 6 reveals that the a-C anode exhibits a high polarization resistance, indicating sluggish charge-transfer kinetics at the anode/electrolyte interface. After 500 cycles, the bulk resistance of a-C increased, whereas that of a-C-Ni decreased. The rise in bulk resistance suggests progressive breakdown of the electrode/electrolyte interface and SEI thickening of a-C during cycling. Conversely, the decrease in bulk resistance of the a-C-Ni anode implies improved electronic conduction and better electrode activation during repeated (de)lithiation processes. Both the a-C and a-C-Ni showed a lower polarization resistance upon cycling, indicating enhanced interfacial charge-transfer kinetics. After cycling, the a-C anode's polarization resistance decreased. Conversely, the a-C-Ni anode showed low polarization resistance, consistent with a prior investigation [25]. Therefore, Ni increased the conductivity of the bulk anodes. The incorporation of Ni additive forms a conductive framework within the amorphous carbon matrix, facilitating electron transport and reducing interfacial impedance.

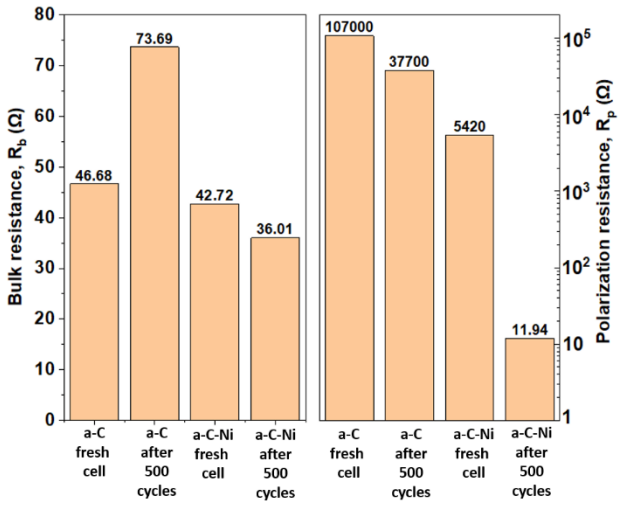


**Figure 6.** Bulk and polarization resistance of a-C and a-C-Ni at different cell conditions

## 4. Conclusion

In this study, we successfully synthesized amorphous carbon via slow pyrolysis at 400 °C using jute stick as the carbon source. We observed a defect-rich, flake-like carbon morphology with exposed porous areas and confirmed a strong $sp^2$-bonded amorphous carbon peak in the FTIR spectra. We performed an electrochemical test by incorporating jute-stick charcoal-mediated carbon as an anode active material in a full cell. The outcomes are summarized as follows:

- The a-C electrode delivered an initial discharge capacity of 137.75 mAh/g and an average discharge capacity of 125.46 mAh/g after 500 cycles at 1C.
- Incorporating 20 wt% Ni increased the initial discharge capacity to 172.27 mAh/g, while the average discharge capacity during the final 50 cycles reached 148.02 mAh/g.
- The a-C-Ni electrode showed an increase in CE from 43.38% in the first cycle to 73% after 500 cycles, indicating improved reversibility during prolonged cycling.
- The cell exhibited reduced bulk and polarization resistance compared with the pristine carbon, indicating that the Ni additive improved electronic conduction and interfacial charge-transfer kinetics.

In conclusion, we prepared a low-cost, facile-fabricated jute-stick charcoal-mediated amorphous carbon anode, and after adding metallic Ni, this electrode delivered improved capacity and cyclic stability. With energy consumption and cost economy as the primary focus, this study introduced a low-cost, facile approach to developing biomass-derived amorphous carbon anodes with improved electrochemical performance through Ni addition. In the future, the possible application of this biomass-derived carbon material and the incorporation of other metallic additives as a sulfur host matrix in Li-S batteries could also be investigated.

**Acknowledgment**

This work is financially supported by the Nanomaterials and Energy Storage System Laboratory (NESS Lab) at the Department of Mechanical Engineering, Chittagong University of Engineering & Technology (CUET), Bangladesh, through research grant no. CUET/CHSR-47.4.4 and CUET/DRE/2025-2026/ME/067.

**Ethical issue**

The authors are aware of and comply with best practices in publication ethics, specifically regarding authorship (avoidance of guest authorship), dual submission, manipulation of figures, competing interests, and compliance with research ethics policies. The authors adhere to publication requirements that the submitted work is original and has not been published elsewhere in any language.

**Data availability statement**

The manuscript contains all the data. However, more data will be available upon request from the corresponding author.

**Conflict of interest**

The authors declare no potential conflict of interest.

**References**

[1] Chandra Bhowmik, K., et al., From Lithium-Ion to Sodium-Ion Batteries for Sustainable Energy Storage: A Comprehensive Review on Recent Research Advancements and Perspectives. The Chemical Record, 2024. 24(12): p. e202400176.

[2] Das, S., Experimental investigation of cycling characteristics of anatase TiO2 nanotubes as negative electrode of lithium-ion batteries. 2023, CUET. http://103.99.128.19:8080/xmlui/handle/123456789/506

[3] Rahman, M.M., et al., Valuation of anode materials for high-performance lithium batteries: From graphite to lithium metal and beyond. Electrochemical Energy Reviews, 2025. 8(1): p. 14.

[4] Wada, H., et al., Graphitization of carbonaceous matter during metamorphism with references to carbonate and pelitic rocks of contact and regional metamorphisms, Japan. Contributions to Mineralogy and Petrology, 1994. 118(3): p. 217–228.

[5] Montiel-García, A., et al., An Overview of the Transition from Amorphous Carbon to an Ordered Graphitic Crystalline Plane for Applications. Materials and Sustainability, 2025. 1(3): p. 12.

[6] Barua, R., K.C. Bhowmik, and M.A. Rahman, Feasibility Study of Basic Steel Slag as Anode of Li-Ion Batteries.

CleanMat, 2026. https://doi.org/10.1002/clem.70038
[7] Huong, D.T., et al., Applying nanocarbon prepared from coal as an anode in lithium-ion batteries. Green Processing and Synthesis, 2025. 14(1): p. 20240151.
[8] Wang, S.-X., et al., Lignin-derived fused electrospun carbon fibrous mats as high performance anode materials for lithium ion batteries. ACS applied materials & interfaces, 2013. 5(23): p. 12275–12282.
[9] Pham, T.L., et al., Synthesis and characterization of porous SiO2/C composite from rice husks through activation with sodium hydroxide and its application in pouch cell Li-ion batteries. 2024. https://doi.org/10.22036/pcr.2024.451396.2511
[10] Jiang, Q., et al., Biomass carbon micro/nano-structures derived from ramie fibers and corncobs as anode materials for lithium-ion and sodium-ion batteries. Applied Surface Science, 2016. 379: p. 73–82.
[11] Han, P., et al., Copper nanoparticle-incorporated carbon fibers as free-standing anodes for lithium-ion batteries. Nanoscale research letters, 2016. 11(1): p. 172.
[12] Yoon, S., et al., Development of a high-performance anode for lithium ion batteries using novel ordered mesoporous tungsten oxide materials with high electrical conductivity. Physical Chemistry Chemical Physics, 2011. 13(23): p. 11060–11066.
[13] Zhang, X., J. Ma, and K. Chen, Impact of morphology of conductive agent and anode material on lithium storage properties. Nano-Micro Letters, 2015. 7(4): p. 360–367.
[14] Ding, W., et al., Nickel-embedded carbon materials derived from wheat flour for Li-Ion storage. Materials, 2020. 13(20): p. 4611.
[15] Nguyen, Q.N., et al., Deciphering energy storage mechanisms and pore structure effects in sugarcane bagasse-derived biomass carbon for lithium–ion batteries and supercapacitors. Biomass and Bioenergy, 2026. 204: p. 108325.
[16] Chen, S., et al., Synthesis of BCN nanoribbons from coconut shells using as high-performance anode materials for lithium-ion batteries. Electrochimica Acta, 2020. 346: p. 136239.
[17] Wang, Q., et al., A waste corn cob core-derived SiO2@ graphene-like carbon nanocomposite and its application in lithium-ion battery. Journal of Materials Science: Materials in Electronics, 2021. 32(1): p. 1278–1288.
[18] Ţucureanu, V., A. Matei, and A.M. Avram, FTIR spectroscopy for carbon family study. Critical reviews in analytical chemistry, 2016. 46(6): p. 502–520.
[19] Benedetti, E., et al., FTIR-microspectroscopy and DSC studies of poly (vinylidene fluoride). Polymer international, 1996. 41(1): p. 35–41.
[20] Buiel, E. and J. Dahn, Li-insertion in hard carbon anode materials for Li-ion batteries. Electrochimica acta, 1999. 45(1-2): p. 121–130.
[21] Yang, F., et al., A study of the relationship between coulombic efficiency and capacity degradation of commercial lithium-ion batteries. Energy, 2018. 145: p. 486–495.
[22] Smith, A.J., et al., Precision Measurements of the Coulombic Efficiency of Lithium-Ion Batteries and of Electrode Materials for Lithium-Ion Batteries. Journal of The Electrochemical Society, 2010. 157(2): p. A196.
[23] Ouyang, H., et al., Porphyra derived hierarchical porous carbon with high graphitization for ultra-stable lithium-ion batteries. Materials Letters, 2019. 235: p. 111–115.
[24] Subrata, K., Impedance spectroscopy for electroceramics and electrochemical system. advanced energy conversion, 2024: p. 10–56.
[25] Soler-Piña, F.J., et al., Highly graphitized carbon nanosheets with embedded Ni nanocrystals as anode for Li-ion batteries. Nano Research, 2020. 13(1): p. 86–94.